SUPPLEMENTAL INFORMATION:

Table of contents:

1. Methods

Mouse genotyping

Mouse genotyping was performed on tail genomic DNA extracted using standard protocols. PCR amplifications were performed across the loxP site of the targeting construct, as well as across the Mut cDNA to detect the INS-MCK-Mut transgene. Primers used were: 5'-loxP site 5'-CCATTCTGGGAAGGCTTCTA-3' and 3'-loxP site 5'-TGCACAGAGTGCTAGTTTCCA-3'. Detection of the INS-MCK-*Mut* transgene was completed by amplification across the *Mut* cDNA with primers: Forward: 5'-CATGTTGAGAGCTAAGAATC-3' and Reverse: 5'-TAGAAGTTCATTCCAATCCC-3'.

Diet and Housing

Mice were housed in a controlled, pathogen-free environment with a 12 hour light/dark cycle and fed ad libitum with standard chow (PicoLab Mouse Diet 20, LabDiet, St. Louis, MO) or a high fat and sugar diet consisting of Diet Induced Obesity Diet (OpenSource Diets™), fruit, and Nutrical® (Tomlyn, Fort Worth, TX). A soft version of the regular chow (Nutra-gel diet, Bio-Serv, Flemington, NJ) was provided for the studies involving AAV administration. For studies involving high protein diet a 70% (wt/wt) casein, or 61% protein chow, (TD.06723, Harlan Laboratories, Madison, WI) was provided ad libitum. Mice were housed on heating strips for thermoneutrality (30^0C) as opposed to regular mouse facility room temperature of 24^0C, to minimize the effects of cold exposure.

In Vivo Stable Isotope Oxidation Studies

Stable isotope studies were performed in 4 *Mut*$^{-/-}$;Tg$^{INS\text{-}MCK\text{-}Mut}$ and 4 control littermates. Closed circuit, constrant volume respiratory chambers were used to collect and measure enrichment of $^{13}CO2$ in mice, as described previously (27, 34). Mice received IP injections with tracer amounts (10µl/g of [1mg/ml] tracer solution) of 99.9% ^{13}C-isotopomers. Aliquots of air were removed every 5-10min, while CO_2 was continuously monitored. $^{1310}CO_3$ enrichment was measured by isotope ratio mass spectroscopy (Metabolic Solutions, Nashua, NH). Results were reported as delta: $\delta = (^{13}C{:}^{12}C_{sample} / {}^{13}C{:}^{12}C_{standard} - 1)*1000$, where Delta C13 units = per mil (‰) = molecules per thousand more than in the standard**.** Cumulative percentage of total isotopomer dose metabolized was subsequently calculated, using the formula: Percentage of dose metabolized = total 13C excreted [mmol/dose (mmol) x 100%].

The following stable isotopes were used: ^{13}C Sodium Propionate, ^{13}C-Methionine, ^{13}C- Glycine, ^{13}C-Pyruvate, ^{13}C-Octanoate, ^{13}C-α-Ketoisocaproic Acid, ^{13}C-Leucine, ^{13}C-Acetate, ^{13}C-Phenylalanine. Stable isotopomers were purchased from Cambridge Isotope Laboratories. Variables were compared for each substrate and time point using a two-sided unpaired t-test and considered statistically significant at $p<0.05$**.**

Clinical Chemistry screen

Murine plasma was obtained terminally by retro-orbital blood collection using heparinized glass capillary tubes (Drummond Scientific, Broomall, PA) following intraperitoneal injection of pentobarbital (5mg/ml, dose of 0.2-0.3 ml/10g body weight). The samples were centrifuged (4^0C, 10 min, 10,000 rpm), the plasma removed, and stored at -80C in a screw-top tube for later analysis. Methylmalonic acid (MMA) was analyzed in plasma and urine samples by gas chromatography-mass spectrometry with stable isotopic calibration as previously described.

MMA values were meaured in patient plasma samples using liquid chromatography–tandem mass spectrometry stable isotope dilution analysis (Mayo Medical Laboratories). Estimated GFR was

calculated using serum creatinine, BUN, and cystatin-C, using the updated CKID equation. 24-hr urine collections were performed in a subset of patients for calculating creatinine clearance (displayed as milliliters per minute per 1.73 m2).

Western Blot, Enzymatic Activity and ELISA assays

Tissue samples were homogenized by tissue grinder in the presence of T-PER and Halt protease inhibitor mixture (both Pierce Biotechnology). Lysates were centrifuged at 10,000 rpm for 10 min at 4 °C, and supernatants were collected. 20 - 30 µg of clarified protein extract were analyzed by Western blot using an affinity-purified, rabbit polyclonal antisera raised against the murine Mut enzyme at a dilution of 1:1,000. The Complex III subunit Core 2 monoclonal antibody was used as a loading control at a dilution of 1:3,000 (MS304; MitoSciences, Eugene, OR). Horseradish peroxidase labeled anti-rabbit IgG (NA934VS; Amersham Biosciences, Piscataway, NJ) or anti-mouse IgG (NA931VS; Amersham) were used as the secondary antibody at a dilution of 1:10,000 or 1:30,000, respectively. Signal was visualized using the SuperSignal West Pico chemiluminescence substrate (34080; Thermo Scientific, Rockford, IL). Protein bands were quantified using ImageJ software (NIH).

To determine mitochondrial respiratory complex activity 40-70 mg of tissue was homogenized in CPT (0.5 M Tris-HCl, 0.15 M KCl; pH 7.5) and centrifuged at 2,500 × g for 20 min at 4 °C. Resulting supernatant was used for protein quantification, detection, and enzymatic activity. 10% extracts of CPT solution were used to measure Complex I activity by oxidation of NADH, and cytochrome c oxidase (COX or complex IV) reduction of cytochrome c at 340 and 550 nm respectively.

Plasma FGF21 concentrations (pg/ml) were measured by quantikine ELISA (DF2100 for human and MF2100 for the mouse assay, R&D Systems and F2131-KO1 for human Intact FGF21, Eagle Biosciences). Specimens, standards and reagents were prepared according to the manufacturer's instructions. All samples were measured in duplicate. Samples above 4,000pg/ml required several serial

dilutions- 10, 20 and 40x - to achieve levels within the reference range. Normal levels according to the manufacturer are for human heparin plasma mean = 186pg/ml, (N = 35, range ND-1012), while for mouse heparin plasma concentrations was 877pg/ml (N = 20, range 283 – 2280). Correlations are presented without measurements for FGF21 over 10,000pg/ml that were originally outside the range of the assay and necessitated serial dilutions to reach an approximated concentration.

Methylmalonyl-CoA mutase (MCM) tissue enzymatic activity by reverse phase HPLC.

Hepatic tissue was cut in pieces, immediately frozen into liquid nitrogen and stored at -80°C until use. On the day of analysis, a small volume (~30 µL) was used to measure protein concentration by the method of Bradford using bovine serum albumin as standard (Bio-Rad protein assay kit, Bio-Rad Laboratories (Canada) Ltd, Mississauga ON, Canada). Then, the remainder of the homogenate was diluted with distilled water to obtain the chosen protein concentration for the assay. A stock solution of methylmalonyl-CoA (1 mM) was prepared in 300 mM of tris-phosphate buffer, pH 7.5; this solution was aliquoted and kept at –30°C. Thus, calibration solutions of methylmalonyl-CoA could be prepared by diluting the stock solution in 100 mmol/L phosphate buffer, pH 4.0. The succinyl-CoA calibration solutions (stock, 500 µM) were prepared in 200 mmol/L phosphoric acid, pH 1.8, aliquoted and stored at –30°C. A solution of AdoCbl (1 mM) for the determination of total enzyme activity was also prepared in distilled water, protected against light inactivation and stored at –30°C. All reagents were purchased from Sigma-Aldrich (Canada Ltd, Oakville, ON, Canada)

The HPLC analyses were carried out on an Agilent technology system consisting of two proStar 210 pumps, 320 UV detector and 420 AutoSampler. The Agilent Poroshell 120 EC-C18, 2.7 µm, 3.0 mm × 100 mm threaded column was heated at 40°C with a HPLC column heater Croco-cil®. The assay reaction mixture for total MCM activity contained, in a total volume of 150 µL, 16 to 333 µg of liver homogenate protein (60 µL), 30 µL of AdoCbl (1 mM), and 60 µL of methylmalonyl-CoA (1 mM). The liver homogenate was first incubated with AdoCbl for 5 minutes at 37°C before initiating the enzyme reaction

by adding methylmalonyl-CoA. The tubes were again incubated at 37°C for 0 to 30 minutes and the reaction was stopped by adding 50 mL of trichloroacetic acid (TCA; 100 g/L). The tubes were centrifuged at 13 000*g* for 1 min. The supernatant was collected and filtered in amber glass vials through a 0.45 µm syringe-operated filter units. A volume of 20 µL of sample was injected in the HPLC system. Blanks were included in every run. The reverse phase column was equilibrated with 56% solvent A (100 mM acetic acid in 100 mM of sodium phosphate buffer, pH 7.0) and 44% solvent B (18% v/v methanol in solvent A). The method consisted in a linear methanol gradient: 0 – 3 min (44% solvent B); 3 – 9 min (44 – 75%); 9 – 12 min (75 – 100%); 12 – 17 min (100 – 44%); and 17 – 35 min (44%) with a flow rate of 0.2 mL/min. The solvent A was filtered through 0.2 µm membrane. The compounds were detected at 254 nm. The optimization and validation of the method was described previously(33) .

Histology, immunohistochemistry and electron microstopy

Tissues for histology were fixed in 10% formalin, embedded into paraffin blocks and subsequently stained with H&E. For immunohistochemistry, liver tissues were snap-frozen in liquid-nitrogen-cooled isopentane. The tissues were cryosectioned and stained for COX and SDH activities, as previously described (82). To visualize histological features and mitochondrial abnormalities, frozen sections of kidney and liver were cut and stained with COX, SDH, and combined COX-SDH reactions. These sections were examined with an Olympus BX51 microscope with a computer-assisted image analysis system. H&E staining was also performed on paraffin sections of various tissues by Histoserv, Inc, Germantown, MD.

Transmission electron microscopy was performed on mouse tissues fixed at 4^0C in 2% glutaraldehyde in 0.1M cacodylate buffer (pH 7.4) and washed with cacodylate buffer. The tissues were fixed with 2% OsO_4 for two hours, washed again with 0.1M cacodylate buffer three times, washed with water and placed in

1% uranyl acetate for one hour. The tissues were subsequently serially dehydrated in ethanol and propylene oxide and embedded in EMBed 812 resin (Electron Microscopy Sciences, Hatfield, PA, USA). Thin sections, approximately 80 nm thick, were obtained by utilizing the Leica ultracut-UCT ultramicrotome (Leica, Deerfield, IL, USA) and placed onto 300 mesh copper grids and stained with saturated uranyl acetate in 50% methanol and then with lead citrate. The grids were viewed in the JEM-1200EXII electron microscope (JEOL Ltd, Tokyo, Japan) at 80 kV and images were recorded on the XR611M, mid mounted, 10.5Mpixel, CCD camera (Advanced Microscopy Techniques Corp, Danvers, MA, USA).

FITC-Inulin Clearance Studies

Glomerular filtration rate (GFR) was assessed by the single-injection FITC-inulin clearance method, as described previously (27). Briefly, serial plasma collections were taken from tail cuts following injection of FITC-inulin and fluorescence measurements of resultant samples were used to determine the rate of decay in comparison to standard curve. Under 1-3% isoflurane anesthesia, mice were given a single bolus retro-orbital injection of 2.5% FITC-inulin (3.74 µl/g body weight). Heparinized blood collections (5 µl volume) from tail cuts were performed at 3, 7, 10, 15, 35, 55, and 75 minutes. Plasma was separated under centrifugation (3 min, 10,000 rpm). Since pH affects FITC fluorescence values, each plasma sample was buffered by mixing 1µl plasma with 9 µl 500 mM HEPES solution (pH 7.4). The amount of FITC label present in the samples was then measured using a fluorospectrometer at 538-nm emission (Thermo Scientific, NanoDrop 3300). A two-compartment clearance model was used to calculate GFR. Plasma fluorescence data were fit to a two-phase exponential decay curve using nonlinear regression (GraphPad Prism, GraphPad Software, San Diego, CA). GFR (µl/min) was calculated using the equation: $GFR = I/(A/\alpha + B/\beta)$, where I is the amount of FITC-inulin delivered by injection, A and B are the y - intercept values of the two decay rates, and α and β are the decay constants for the distribution and elimination phases, respectively (83, 84).

Microarray experiments

For transcriptome analysis liver tissue RNA expression was studied in livers from the following 4 conditions: heterozygote *Mut* $^{+/-}$;Tg$^{\text{INS-MCK-}Mut}$ mice at baseline and after 12 hrs of fasting, mutant *Mut* $^{-/-}$;Tg$^{\text{INS-MCK-}Mut}$ mice at baseline and after 8-12 hrs of fasting. Four mice in each genotype group and fed or fasting state were sacrificed for liver and RNA extraction. All the mice used in this study were males, at 4 months of age. After organ removal, livers were snap frozen in liquid nitrogen. Total RNA from liver tissue was extracted using the RNA mini kit (74104 Qiagen). cDNA was labeled by the GeneChip Ambion WT expression kit for 1.0 ST chips (4411973; Ambion) and hybridized to Affymetrix GeneChip Mouse Gene 1.0ST Arrays (901168; Affymetrix) according to the manufacturer's instructions. Data were analyzed using Partel Genomics Suite software (Partek) and pathway analysis was coducted using Ingenuity Pathway analysis (Ingenuity Systems).

Principal component analysis was performed generating histograms to assess the biological variability of the microarrays. Using hierarchical cluster analysis, the transcriptomes of the 4 different groups of mice showed satisfactory segregation and differential clustering. Baseline, non-fasting mutant mice showed the lower co-segregation, as expected, given their mixed, non-standardized dietary composition (regular chow, supplemented by fruit/enercal and high fat, for caloric suport).

To investigate biological patterns, we performed canonical pathway enrichment analysis using the Ingenuity Pathway Analysis Pathway (QIAGEN bioinformatics, Redwood City 1700 Seaport Blvd #3 Redwood City CA 94063) and calculated a P value for each pathway that was adjusted for multiple testing using the Benjamini-Hochberg method. A P-value of 0.05 after correcting for multiple comparisons was used to determine statistical significant changes.

The microarray data were deposited in Gene Epxression Omnibus (GEO) database (accession No: GSE118862).

Quantitative real-time PCR analysis. Total RNA from frozen tissue was extracted using the RNeasy Mini Kit (74104; Quiagen, Valencia, CA). DNase digestion was performed using DNA-free (AM1906; Ambion, Austin, TX) and 2μg of RNA was reverse transcribed using the High Capacity cDNA Kit (4368814; Applied Biosystems, Foster City, CA). Taqman gene expression assays were performed in triplicate according to the manufacturer's instructions using the Fast-Universal PCR Master Mix (4352042, Applied Biosystems) and the Applied Biosystems 7500 Fast Real-Time PCR System. TaqMan probes specific to selected genes were used and listed in Supplemental Table 3 (Applied Biosystems. Foster City, CA). mRNA expression levels were normalized to GAPDH (Mm99999915_g1; Applied Biosystems) and quantification of relative gene expression, presented as percentage of the relevant baseline, was calculated using the 2^-[delta][delta]CT (comparative threshold) method.

2. Figures

Supplemental Figure 1.

Generation of the *Mut*$^{-/-}$;Tg$^{INS\text{-}MCK\text{-}Mut}$ murine model.

(A) Schematic representation of the *Mut* knockout allele and the INS-MCK-*Mut* construct used to produce the transgenic model, *Mut*$^{-/-}$;Tg$^{INS\text{-}MCK\text{-}Mut}$. (**B**) Quantitative RT-PCR analysis of *Mut* mRNA expression in the muscle and liver. Results are provided as percentage of the levels obtained in wild-type (*Mut*$^{+/+}$) animals, corrected for *Gapdh* expression (mean ± SEM; n = 3–5; P = 0.0027). The muscle *Mut* mRNA expression from the transgene was 19,492.5 ± 2,962.5 % and the heart was 2,654 ± 1666 % compared to their *Mut*$^{+/+}$ littermates (*P*=0.0027, N=5) , while there was no detectable Mut mRNA in the liver (0.0928 ± 0.04 % compared to wild type), kidney or brain tissues. (**C**) Mut (78 kDa) was detected in whole-tissue lysates from *Mut*$^{-/-}$;Tg$^{INS\text{-}MCK\text{-}Mut}$ muscle and heart, but not in liver, kidney or brain protein extracts. The Complex III subunit Core 2 used as a loading control indicates that 15-fold less protein was loaded for the muscle tissue in order to obtain a regular size band after chemiluminescence, because of the strength of the signal. (**D**) The liver transgenic model (*Mut*$^{-/-}$;Tg$^{INS\text{-}Alb\text{-}Mut}$) exhibits significant higher percent control propionate oxidation (78.04 ± 22.1% control) compared to the *Mut*$^{-/-}$;Tg$^{INS\text{-}MCK\text{-}Mut}$ mice (36.2 ± 7.1% control, *P*=0.0007). (**E**) At 3-4 mo of age, *Mut*$^{-/-}$;Tg$^{INS\text{-}MCK\text{-}Mut}$ mice appear active and well, but are consistently smaller than heterozygote littermates, whether fed regular chow or a high fat and carbohydrate diet.

Supplemental Figure 2.

Hepatic pathological and ultrastructural changes in Mut$^{-/-}$;Tg$^{INS\text{-}MCK\text{-}Mut}$ animals and MMA patients

(A) Hepatic pathology in mutant mice (panel b) was notable for swollen hepatocytes with increased eosinophilia and scattered Mallory bodies (inset, panel b). Hepatocytes contained numerous cytoplasmic eosinophilic vacuoles consistent with megamitochondria (yellow arrow, panel c). Steatosis was observed

in heterozygote animals reared on the same high fat and carbohydrate diet (panel a). No significant disruption of hepatic lobe architecture, fibrotic or cirrhotic changes were observed. Hematoxylin and eosin staining of liver sections from a 4-month-old mouse are shown, scale bars: 20-100µm). (**B**) Explanted livers from patients undergoing a liver transplantation displayed mostly macrovesicular periportal steatosis, with lipid ladden stellate cells (panel b, yellow arrowhead) and occasional lipofuscin pigment granules (inset, panel b). Mitochondria with a reduction or loss of matrix density, unusual size/shape and shortened, disorganized cristae are invariably present in liver pathology examinations by electron microscopy (B, panels d-h). In some patients, liver ultrastructure revealed complex cytoplasmic structures with inclusions of various size and density engulfed by membranes suggestive of autophagosomes (B, panel i).

Supplemental Figure 3.

Hepatic mitochondrial dysfunction.

(**A**) Immunohistochemistry for Cox and Sdh on liver section of mutant mice revealed significantly decrease in Cox staining (10x) compared to the heterozygote littermates. (**B**) Cytochrome c oxidase enzymatic activity in the livers of the *Mut*$^{-/-}$;Tg$^{\text{INS-MCK-}Mut}$ mice were significantly lower than control mice, and similar to the *Mut*$^{-/-}$ livers (n=3 per group). (**C** and **D**) Cumulative percentage of total isotopomer dose metabolized in 30min after intraperitoneal injection of a tracer dose (10µl/g of [1mg/ml] tracer solution) is depicted for methionine and glycine 1-^{13}C isotopomer. Oxidation of both amino acids was perturbed in the *Mut*$^{-/-}$;Tg$^{\text{INS-MCK-}Mut}$ mice compared to their heterozygote littermates consistent with impaired activity of the glycine cleavage system and the mitochondrial steps of methionine metabolism caused by a shift in the NAD:NADH balance in the mitochondria.

Supplemental Figure 4.

Renal pathology in *Mut*$^{-/-}$;Tg$^{\text{INS-MCK-}Mut}$ mice.

(**A**) Renal pathology showed mild interstitial nephritis and tubular vacuoles (white arrow) with accumulation of pigment in some proximal tubules' brush border (scale bars: 20mm, panel a). On electron microscopy, proximal tubules showed increased number of abnormally shaped mitochondria with decreased matrix density as opposed to their heterozygote littermates (scale bars: 1mm, panel b and c). (**B**) Plasma Lipocalin-2 (Lcn2) concentrations were elevated in *Mut*$^{-/-}$;Tg$^{\text{INS-MCK-}Mut}$ mice on regular chow at 4-5 months of age compared to their heterozygote littermates (129.1 ± 22.09ng/ml vs 75.21 ± 6.41, n=6 each group, P=0.0413). (**C**) Plasma Lcn2 showed a negative trend with the glomerular filtration rate measured by the FITC inulin plasma decay method (r = -0.661, R^2= 0.45, P=0.10).

Supplemental Figure 5.

Biochemical and other findings in *Mut*$^{-/-}$;Tg$^{\text{INS-MCK-}Mut}$ mice.

(**A**) Serum chemistries, including BUN, liver function testing, amylase, CK and LDH. Significant differences we only observed in alkaline phosphatase and amylase levels between *Mut*$^{-/-}$;Tg$^{\text{INS-MCK-}Mut}$ mice and their heterozygote littermates. (**B**) Two-hour glucose tolerance test in *Mut*$^{-/-}$;Tg$^{\text{INS-MCK-}Mut}$ mice, showed no difference in glucose control from heterozygote littermates on the same high fat/carbohydrate diet. (**C**) Hematoxylin-eosin stain of the quadriceps muscle shows no abnormal findings in *Mut*$^{-/-}$;Tg$^{\text{INS-MCK-}Mut}$ mice.

Supplemental Figure 6.

Fasting challenge.

(**A**) Blood glucose monitoring during the overnight fasting study in male and female *Mut*$^{-/-}$;Tg$^{\text{INS-MCK-}Mut}$ mice detected hypoglycemia in the smaller female mice between 15-16hrs of fasting. Mice were euthanized for tissue collection at this time point. (**B**) The dendrogram represents hierarchical clustering of genes with similar expression pattern in the microarray experiments in liver tissues. Genes upregulated in the *Mut*$^{-/-}$;Tg$^{\text{INS-MCK-}Mut}$ mice as opposed to control animals are indicated in Red and

downregulated in Blue. Microarrays were performed in 2 groups of animals, mutant and control mice, in two conditions, baseline and fasting states. The scale (red to blue) represents the ratios of differential expression based on signal intensity.

Longitudinal Fgf21 values: (**C**) Samples obtained in a small number over time suggest that values are higher at weaning, even for some heterozygote animals, and then gradually increase after the first month in the *Mut*$^{-/-}$;Tg$^{\text{INS-MCK-}Mut}$ transgenic mice.

Supplemental Figure 7.

Validation of selected up- and down-regulated genes in the microarray experiment

Hepatic expression of selected genes in the unfasted and fasted state in heterozygote and mutant animals is depicted. An exaggerated response was often seen in *Mut*$^{-/-}$;Tg$^{\text{INS-MCK-}Mut}$ mice in several pathways (for example: *Gadd45b, Pdk4*), while for others a divergent response was observed, with genes that are normally downregulated being significantly induced (*Gstm3, Slc7A11, Rragd).* Downregulation of *Fasn* and *Hsd3b2* was consistent between *Mut*$^{-/-}$;Tg$^{\text{INS-MCK-}Mut}$ and their heterozygote littermates.

Supplemental Figure 8.

Plasma total and intact FGF21 and correlations with other biochemical parameters.

(A) Total and intact (active) FGF21 were measured in the same samples (N=38). Intact FGF21 ranged from 33.92 to 18,235 pg/ml (2,262 ± 3,636, mean ± SD). (B) Delta Total-Intact FGF21 showed a weak correlation (R^2=0.18, r=0.42, P=0.014) with renal function. (C) Serial FGF21 measurements before, during and after a metabolic crisis in two MMA siblings showed massive temporary increases in serum FGF21 concentrations that returned to pre-crisis levels upon recovery. (D) Plasma FGF21 correlated positively with plasma amino acids (glycine: r=0.36, P=0.0227, R^2=0.132 and alanine: r=0.41, P=0.0079,

R^2=0.175, solid circles vs. clear square symbols, respectively), as well as (E) with urinary F2-isoprostanes (*r*=0.39, *P*=0.03, R^2=0.154). (F) There was a negative correlation with plasma valine (*r*=-0.345, *P*=0.03, R^2=0.12).

3. Tables:

Supplemental Table 1. Differentially expressed genes. Fold change (+/- 2.5-fold or higher) in mRNA expression of mutant vs. heterozygous mice in the fasting state.

Highlighted genes were validated by RT-PCR, see Supplemental Figure 7.

Gene ID	Gene name description	Fold change
Up-regulated in *Mut*$^{-/-}$;Tg$^{INS\text{-}MCK\text{-}Mut}$		
Cyp2b13	cytochrome P450, family 2, subfamily b, polypeptide 13	17.220
Lepr	leptin receptor	13.693
Cyp2b9	cytochrome P450, family 2, subfamily b, polypeptide 9	11.378
Slc7a11	solute carrier family 7 (cationic amino acid transporter, y+ system), member 11	11.193
Cyp2a22	cytochrome P450, family 2, subfamily a, polypeptide 22	8.403
Asns	asparagine synthetase (glutamine-hydrolyzing)	7.674
Aqp7	aquaporin 7	6.147
Gstm3	glutathione S-transferase, mu 3	5.765
Prss8	protease, serine 8 (prostasin)	5.134
Abcc4	ATP-binding cassette, sub-family C (CFTR/MRP), member 4	4.627
Cd63	CD63 antigen	4.570
Socs2	suppressor of cytokine signaling 2	4.520
Serpina7	serine (or cysteine) peptidase inhibitor, clade A (alpha-1 antiproteinase, antitrypsin), member 7	4.246
Fmo3	flavin containing monooxygenase 3	4.245
Fabp5	fatty acid binding protein 5, epidermal	4.162
Myc	myelocytomatosis oncogene	3.962
Ly6d	lymphocyte antigen 6 complex, locus D	3.910
Psat1	phosphoserine aminotransferase 1	3.901
Itga6	integrin alpha 6	3.876
Nipal1	NIPA-like domain containing 1	3.718
Prrg4	proline rich Gla (G-carboxyglutamic acid) 4 (transmembrane)	3.709
Slc35f2	solute carrier family 35, member F2	3.681

Ucp2	uncoupling protein 2 (mitochondrial, proton carrier)	3.610
Fabp5	fatty acid binding protein 5, epidermal	3.585
Nupr1	nuclear protein transcription regulator 1	3.570
Acot2	acyl-CoA thioesterase 2	3.569
Usp18	ubiquitin specific peptidase 18	3.429
Ccnd1	cyclin D1	3.408
Tuba8	tubulin, alpha 8	3.328
Car2	carbonic anhydrase 2	3.317
Slc7a11	solute carrier family 22 (organic cation transporter), member 26	3.317
Pdk4	pyruvate dehydrogenase kinase, isoenzyme 4	3.095
Cpt1b	carnitine palmitoyltransferase 1b, muscle	3.087
Ntf3	neurotrophin 3	3.057
Abcd2	ATP-binding cassette, sub-family D (ALD), member 2	3.041
Hmox1	heme oxygenase 1	2.994
Sqle	squalene epoxidase	2.967
Slc22a27	solute carrier family 22, member 27	2.927
Rragd	Ras-related GTP binding D	2.899
S100a11	S100 calcium binding protein A11	2.847
Cyp11b1	cytochrome P450, family 11, subfamily b, polypeptide 1	2.814
Vldlr	very low density lipoprotein receptor	2.811
Cln6	ceroid-lipofuscinosis, neuronal 6	2.737
App	amyloid beta (A4) precursor protein	2.694
Dhrs9	dehydrogenase/reductase (SDR family) member 9	2.682
Pfkp	phosphofructokinase, platelet	2.661
Acsl4	acyl-CoA synthetase long-chain family member 4	2.651
Fabp3	fatty acid binding protein 3, muscle and heart	2.631
Sgk1	serum/glucocorticoid regulated kinase 1	2.627
Renbp	renin binding protein	2.592
Adra2a	adrenergic receptor, alpha 2a	2.550
Morc4	microrchidia 4	2.500
Fgf21	*Fibroblast growth factor 21*	*1.519*

Down-regulated in *Mut*$^{-/-}$;Tg$^{\text{INS-MCK-}Mut}$

Elovl3	elongation of very long chain fatty acids (FEN1/Elo2, SUR4/Elo3, yeast)-like 3	-13.414
Orm1	orosomucoid 1	-12.533
Nnmt	nicotinamide N-methyltransferase	-10.919
Slco1a1	solute carrier organic anion transporter family, member 1a1	-9.778
Obp2a	odorant binding protein 2A (*Lcn13*)	-8.909
Slc3a1	solute carrier family 3, member 1	-8.471
C9	complement component 9	-7.428
Pigr	polymeric immunoglobulin receptor	-6.746

Orm3	orsomucoid 3	-6.603
Saa2	serum amyloid A 2	-6.538
Cyp7b1	cytochrome P450, family 7, subfamily b, polypeptide 1	-4.891
Ces3b	carboxylesterase 3B	-4.631
Hsd3b2	hydroxy-delta-5-steroid dehydrogenase, 3 beta- and steroid delta-isomerase 2	-3.886
Ido2	indoleamine 2,3-dioxygenase 2	-3.459
Mut	methylmalonyl-Coenzyme A mutase	-3.448
Susd4	sushi domain containing 4	-3.285
Saa4	serum amyloid A 4	-3.257
Mup3	major urinary protein 3	-3.209
Slc8a1	solute carrier family 8 (sodium/calcium exchanger), member 1	-3.193
C6	complement component 6	-3.113
Sucnr1	succinate receptor 1	-2.997
Scnn1a	sodium channel, nonvoltage-gated 1 alpha	-2.989
Alas2	aminolevulinic acid synthase 2, erythroid	-2.893
P2ry4	pyrimidinergic receptor P2Y, G-protein coupled, 4	-2.842
Car1	carbonic anhydrase 1	-2.820
Abat	4-aminobutyrate aminotransferase	-2.788
Acnat2	acyl-coenzyme A amino acid N-acyltransferase 2	-2.788
Nox4	NADPH oxidase 4	-2.769
Arrdc3	arrestin domain containing 3	-2.762
Mbl2	mannose-binding lectin (protein C) 2	-2.747
Fam55b	neurexophilin and PC-esterase domain family, member 2	-2.710
Cyp2c54	cytochrome P450, family 2, subfamily c, polypeptide 54	-2.651
Nr0b2	nuclear receptor subfamily 0 group B member 2	-2.617
Hsd3b5	hydroxy-delta-5-steroid dehydrogenase, 3 beta- and steroid delta-isomerase 5	-2.614
Fitm1	fat storage-inducing transmembrane protein 1	-2.614
Cyp2d9	cytochrome P450, family 2, subfamily d, polypeptide 9	-2.584
Cyp2u1	cytochrome P450, family 2, subfamily u, polypeptide 1	-2.561
Srd5a1	steroid 5 alpha-reductase 1	-2.554
Bdh2	3-hydroxybutyrate dehydrogenase, type 2	-2.529
Mfsd2a	major facilitator superfamily domain containing 2A	-2.528
Hsd3b3	hydroxy-delta-5-steroid dehydrogenase, 3 beta- and steroid delta-isomerase 3	-2.501

Supplemental Table 2. Differentially expressed genes. Fold change (+/- 2.5-fold or higher) in mRNA expression of mutant vs. heterozygous mice at baseline.

Highlighted genes were validated by RT-PCR, see Supplemental Figure 7.

Gene ID	Gene name description	Fold change
Up-regulated in *Mut*$^{-/-}$;Tg$^{INS\text{-}MCK\text{-}Mut}$		
Cyp2b13	cytochrome P450, family 2, subfamily b, polypeptide 13	22.737
Cyp2b9	cytochrome P450, family 2, subfamily b, polypeptide 9	15.493
Cyp2a22	cytochrome P450, family 2, subfamily a, polypeptide 22	12.580
Slc7a11	solute carrier family 7 (cationic amino acid transporter, y+ system), member 11	10.993
Igfbp1	insulin-like growth factor binding protein 1	7.027
Asns	asparagine synthetase (glutamine-hydrolyzing)	6.168
Lepr	leptin receptor	5.876
Mt1	metallothionein 1	5.876
Mt2	metallothionein 2	5.795
Fmo3	flavin containing monooxygenase 3	5.301
Pdk4	pyruvate dehydrogenase kinase, isoenzyme 4	4.696
Abcd2	ATP-binding cassette, sub-family D (ALD), member 2	4.688
Abcc4	ATP-binding cassette, sub-family C (CFTR/MRP), member 4	4.444
Aqp7	aquaporin 7	4.362
Cdkn1a	cyclin-dependent kinase inhibitor 1A (P21)	4.303
Lcn2	lipocalin 2	4.039
Slc16a5	solute carrier family 16 member 5	4.003
Cyp39a1	cytochrome P450, family 39, subfamily a, polypeptide 1	3.985
Acot2	acyl-CoA thioesterase 2	3.893
Serpina7	serine (or cysteine) peptidase inhibitor, clade A	3.837
Gstm3	glutathione S-transferase, mu 3	3.793
Fmo2	flavin containing monooxygenase 2	3.768
Ccnd1	cyclin D1	3.642
Atp6v0d2	ATPase, H+ transporting, lysosomal V0 subunit D2	3.617
Tuba8	tubulin, alpha 8	3.534
Itga6	integrin alpha 6	3.505
Prss8	protease, serine, 8 (prostasin)	3.494
Ucp2	uncoupling protein 2 (mitochondrial, proton carrier)	3.475
Agpat9	1-acylglycerol-3-phosphate O-acyltransferase 9	3.419

Nipal1	NIPA-like domain containing 1	3.386
Prrg4	proline rich Gla (G-carboxyglutamic acid) 4	3.268
Gadd45b	growth arrest and DNA-damage-inducible 45 beta	3.207
Fgf21	fibroblast growth factor 21	3.202
Vldlr	very low density lipoprotein receptor	3.160
Rragd	Ras-related GTP binding D	3.135
Slc35f2	solute carrier family 35, member F2	3.093

Down-regulated in *Mut*$^{-/-}$;Tg$^{\text{INS-MCK-}Mut}$

Hsd3b5	hydroxy-delta-5-steroid dehydrogenase, 3 beta	-38.006
Serpina4-ps1	serine (or cysteine) peptidase inhibitor, clade A, member 4, pseudogene 1	-33.691
Elovl3	elongation of very long chain fatty acids (FEN1/Elo2, SUR4/Elo3, yeast)-like 3	-17.967
Lcn13	lipocalin 13	-13.401
Orm1	orosomucoid 1	-8.209
Slco1a1	solute carrier organic anion transporter family, member	-7.999
Cyp7b1	cytochrome P450, family 7, subfamily b, polypeptide 1	-6.793
Mup21	major urinary protein 21	-6.245
Slc10a2	solute carrier family 10, member 2	-5.079
C9	complement component 9	-4.834
Gm4738	predicted gene 4738	-4.695
Slc3a1	solute carrier family 3, member 1	-4.560
Cyp2u1	cytochrome P450, family 2, subfamily u, polypeptide 1	-4.528
Pigr	polymeric immunoglobulin receptor	-4.351
Dpy19l3	dpy-19-like 3 (C. elegans)	-4.330
Ust	uronyl-2-sulfotransferase	-3.963
Nnmt	nicotinamide N-methyltransferase	-3.930
c	predicted gene 4956	-3.912
Hsd3b2	hydroxy-delta-5-steroid dehydrogenase, 3 beta- and steroid delta-isomerase 2	-3.873
Cyp8b1	cytochrome P450, family 8, subfamily b, polypeptide 1	-3.834
C6	complement component 6	-3.662
Srd5a1	steroid 5 alpha-reductase 1	-3.631
Mut	methylmalonyl-Coenzyme A mutase	-3.406
Gm11437	predicted gene 11437	-3.338
Adh6-ps1	alcohol dehydrogenase 6 (class V), pseudogene 1	-3.277
Agxt2l1	alanine-glyoxylate aminotransferase 2-like 1	-3.040
Sucnr1	succinate receptor 1	-3.013

Supplemental Table 3: TaqMan probes for quantitative PCR validation of differentially expressed genes identified by microarray expression analysis

(presented in supplemental figure 7)

Gene ID	Gene name description	Taqman probe
Fgf21	Fibroblast growth factor 21	Mm00840165_g1
Gadd45b	growth arrest and DNA-damage-inducible 45 beta	Mm00435123_m1
Pdk4	pyruvate dehydrogenase kinase, isoenzyme 4	Mm01166879_m1
Gstm3	glutathione S-transferase, mu 3	Mm00833923_m1
Slc7a11	solute carrier family 7 (cationic amino acid transporter, y+ system), member 11	Mm00442530_m1
Rragd	Ras-related GTP binding D	Mm00546741_m1
Socs2	suppressor of cytokine signaling 2	Mm00850544_g1
Asns	asparagine synthetase (glutamine-hydrolyzing)	Mm00803785_m1
Lepr	leptin receptor	Mm00440181_m1
Abcc4	ATP-binding cassette, sub-family C (CFTR/MRP), member 4	Mm01226381_m1
Fasn	fatty Acid synthase	Mm00662319_m1
Hsd3b2	hydroxy-delta-5-steroid dehydrogenase, 3 beta- and steroid delta-isomerase 2	Mm00462685_m1

Supplemental Figure 1

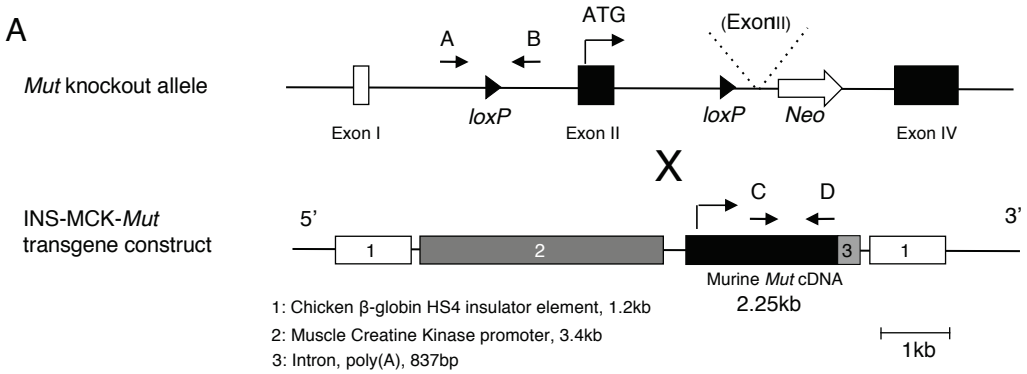

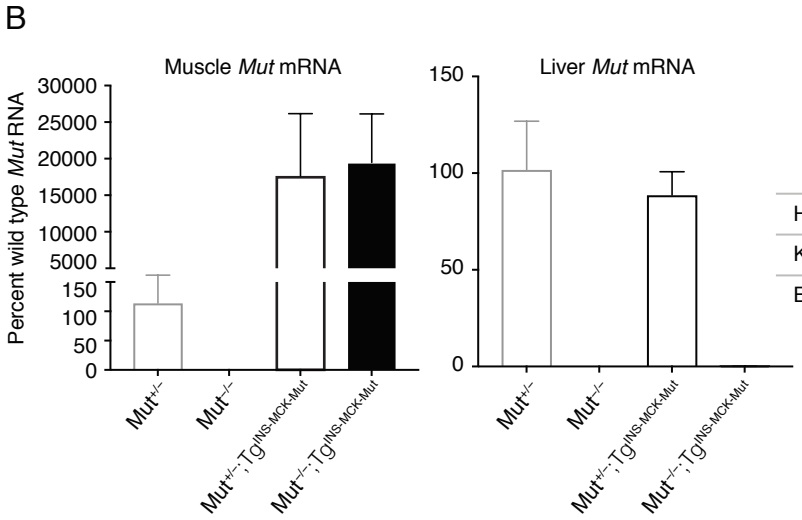

	Mut +/–; TgINS-MCK-Mut	Mut –/–; TgINS-MCK-Mut
Heart	3755 ± 1658	2654 ± 1666
Kidney	97 ± 16	0.04 ± 0.05
Brain	228 ± 128	6.4 ± 0.5

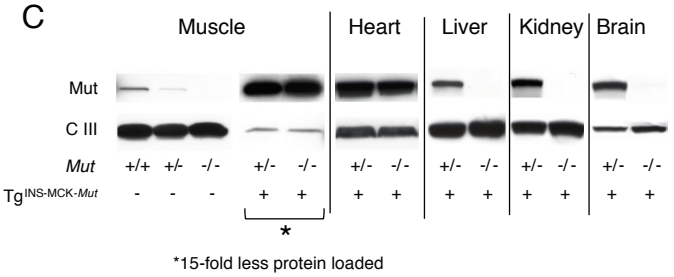

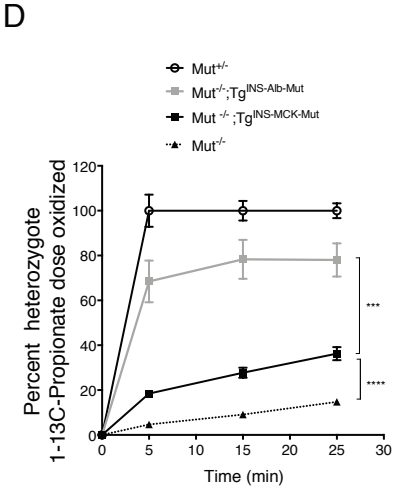

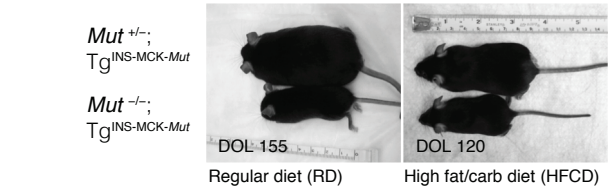

Generation of the *Mut*$^{-/-}$;Tg$^{INS\text{-}MCK\text{-}Mut}$ murine model.
(A) Schematic representation of the Mut knockout allele and the INS-MCK-Mut construct used to produce the transgenic model, ***Mut*** $^{-/-}$;Tg$^{INS\text{-}MCK\text{-}Mut}$. **(B)** Quantitative RT-PCR analysis of ***Mut*** mRNA expression in the muscle and liver. Results are provided as percentage of the levels obtained in wild-type (***Mut***$^{+/+}$) animals, corrected for Gapdh expression (mean ± SEM; n = 3–5; P = 0.0027). The muscle ***Mut*** mRNA expression from the transgene was 19,492.5 ± 2,962.5 % and the heart was 2,654 ± 1666 % compared to their ***Mut***$^{+/+}$ littermates(*P*=0.0027, N=5) , while there was no detectable ***Mut*** mRNA in the liver (0.0928 ± 0.04 % compared to wild type), kidney or brain tissues. **(C)** Mut (78 kDa) was detected in whole-tissue lysates from ***Mut***$^{-/-}$;Tg$^{INS\text{-}MCK\text{-}Mut}$ muscle and heart, but not in liver, kidney or brain protein extracts. The Complex III subunit Core 2 used as a loading control indicates that 15-fold less protein was loaded for the muscle tissue in order to obtain a regular size band after chemiluminescence, because of the strength of the signal. **(D)** The liver transgenic model (***Mut***$^{-/-}$;Tg$^{INS\text{-}MCK\text{-}Mut}$) exhibits significant higher percent control propionate oxidation (78.04 ± 22.1% control) compared to the ***Mut***$^{-/-}$;Tg$^{INS\text{-}MCK\text{-}Mut}$ mice (36.2 ± 7.1% control, *P*=0.0007). **(E)** At 3-4 mo of age, ***Mut***$^{-/-}$;Tg$^{INS\text{-}MCK\text{-}Mut}$ mice appear active and well, but are consistently smaller than heterozygote littermates, whether fed regular chow or a high fat and carbohydrate diet.

Supplemental Figure 2

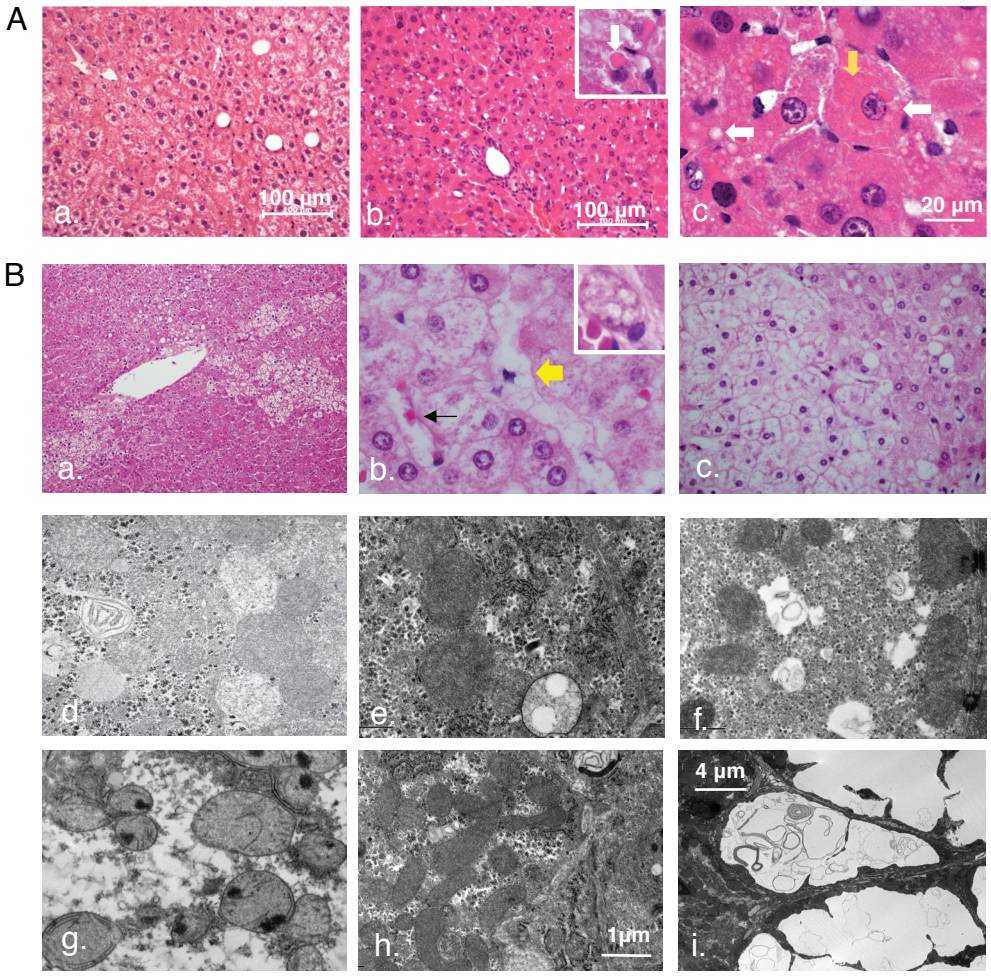

Hepatic pathological and ultrastructural changes in Mut$^{-/-}$;Tg$^{INS\text{-}MCK\text{-}Mut}$ animals and MMA patients
(A) Hepatic pathology in mutant mice (panel b) was notable for swollen hepatocytes with increased eosinophilia and scattered Mallory bodies (inset, panel b). Hepatocytes contained numerous cytoplasmic eosinophilic vacuoles consistent with megamitochondria (yellow arrow, panel c). Steatosis was observed in heterozygote animals reared on the same high fat and carbohydrate diet (panel a). No significant disruption of hepatic lobe architecture, fibrotic or cirrhotic changes were observed. Hematoxylin and eosin staining of liver sections from a 4-month old mice are shown, scale bars: 20-100µm).(**B**) Explanted livers from patients undergoing a liver transplantation displayed mostly macrovesicular periportal steatosis, lipid ladden stellate cells (panel b, yellow arrowhead) and occasional lipofuscin pigment granules (inset, panel b). Mitochondria with a reduction or loss of matrix density, unusual size/shape and shortened, disorganized cristae are invariably present in liver pathology examinations by electron microscopy (B, panels d-h). In some patients, liver ultrastructure revealed complex cytoplasmic structures with inclusions of various size and density engulfed by membranes suggestive of autophagosomes (B, panel i).

Supplemental Figure 3

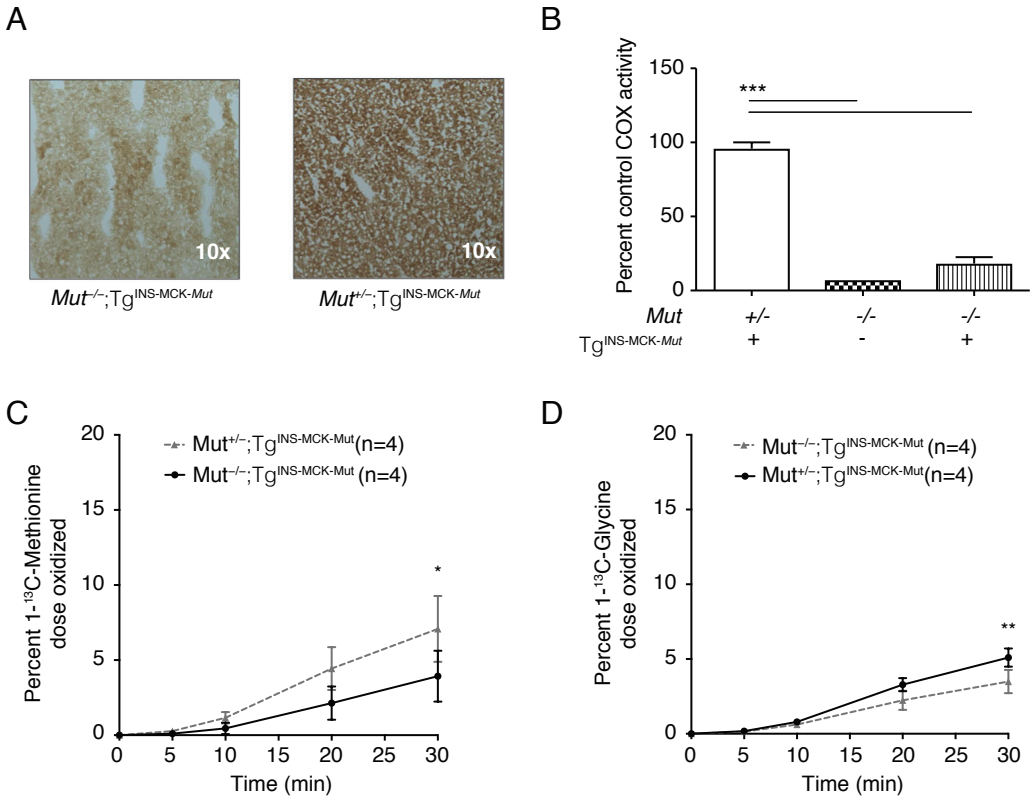

Hepatic mitochondrial dysfunction.
(**A**) Immunohistochemistry for Cox and Sdh on liver section of mutant mice revealed significantly decrease in Cox staining (10x) compared to the heterozygote littermates. (**B**) Cytochrome c oxidase enzymatic activity in the livers of the *Mut*$^{-/-}$;Tg$^{INS\text{-}MCK\text{-}Mut}$ mice were significantly lower than control mice, and similar to the *Mut*$^{-/-}$ livers (n=3 per group). (**C** and **D**) Cumulative percentage of total isotopomer dose metabolized in 30min after intraperitoneal injection of a tracer dose (10μl/g of [1mg/ml] tracer solution) is depicted for methionine and glycine 1-^{13}C isotopomer. Oxidation of both amino acids was perturbed in the *Mut*$^{-/-}$;Tg$^{INS\text{-}MCK\text{-}Mut}$ mice compared to their heterozygote littermates consistent with impaired activity of the glycine cleavage system and the mitochondrial steps of methionine metabolism caused by a shift in the NAD:NADH balance in the mitochondria.

Supplemental Figure 4

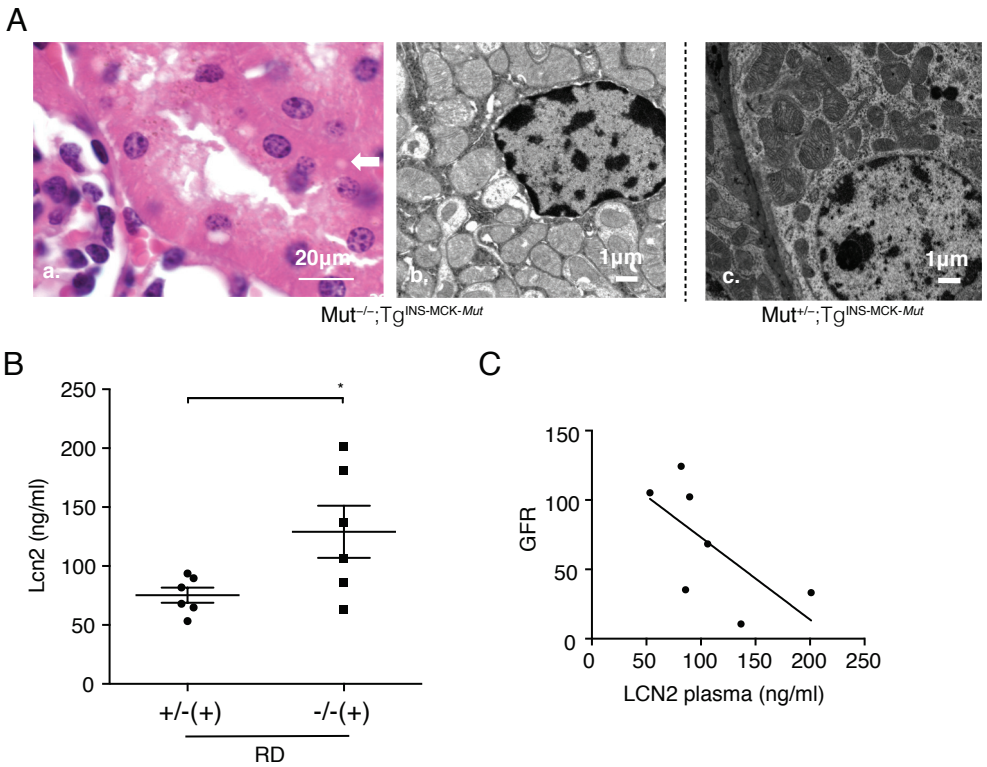

Renal pathology in *Mut*$^{-/-}$;Tg$^{INS\text{-}MCK\text{-}Mut}$ mice.
(**A**) Renal pathology showed mild interstitial nephritis and tubular vacuoles (white arrow) with accumulation of pigment in some proximal tubules' brush border (scale bars: 20µm, panel a). On electron microscopy, proximal tubules showed increased number of abnormally shaped mitochondria with decreased matrix density as opposed to their heterozygote littermates (scale bars: 1µm, panel b and c). (**B**) Plasma Lipocalin-2 (Lcn2) concentrations were elevated in *Mut*$^{-/-}$;Tg$^{INS\text{-}MCK\text{-}Mut}$ mice on regular chow at 4-5 months of age compared to their heterozygote littermates (129.1 ± 22.09ng/ml vs 75.21 ± 6.41, n=6 each group, P=0.0413). (**C**) Plasma Lcn2 showed a negative trend with the glomerular filtration rate measured by the FITC inulin plasma decay method (r = -0.661, R^2= 0.45, P=0.10).

Supplemental Figure 5

A

Serum Chemistries	$Mut^{+/-};Tg^{INS\text{-}MCK\text{-}Mut}$		$Mut^{-/-};Tg^{INS\text{-}MCK\text{-}Mut}$		
	mean	SD	mean	SD	*P*-value
BUN	14.8	2.6	14.5	4.1	0.862
Alkaline Phos.	56.4	16.8	107.8	35.1	**0.009**
ALT/GPT	24.2	10.7	26.7	9.0	0.671
AST/GOT	53.1	20.4	55.6	36.0	0.883
Amylase	1614.7	512.3	1008.8	381.1	**0.042**
CK	384.1	666.2	238.9	307.2	0.638
LDH	478.3	144.1	580.0	365.2	0.540

B

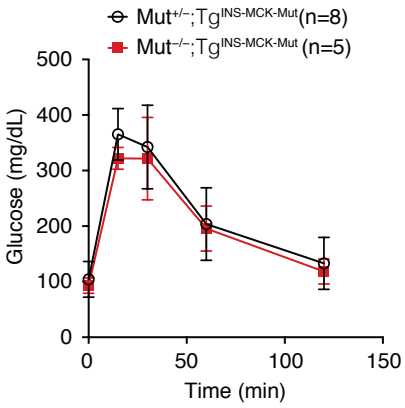

C

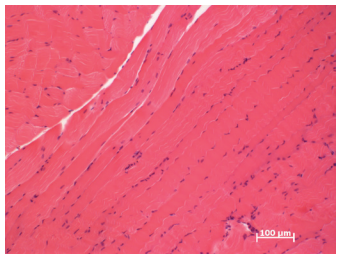

Biochemical and other findings in $Mut^{-/-};TgINS\text{-}MCK\text{-}Mut$ mice.
(**A**) Serum chemistries, including BUN, liver function testing, amylase, CK and LDH. Significant differences we only observed in alkaline phosphatase and amylase levels between $Mut^{-/-}$;TgINS-MCK-Mut mice and their heterozygote littermates. (**B**) Two-hour glucose tolerance test in $Mut^{-/-}$;TgINS-MCK-Mut mice, showed no difference in glucose control from heterozygote littermates on the same high fat/carbohydrate diet. (**C**) Hematoxylin-eosin stain of the quadriceps muscle shows no abnormal findings in $Mut^{-/-}$;TgINS-MCK-Mut mice.

Supplemental Figure 6

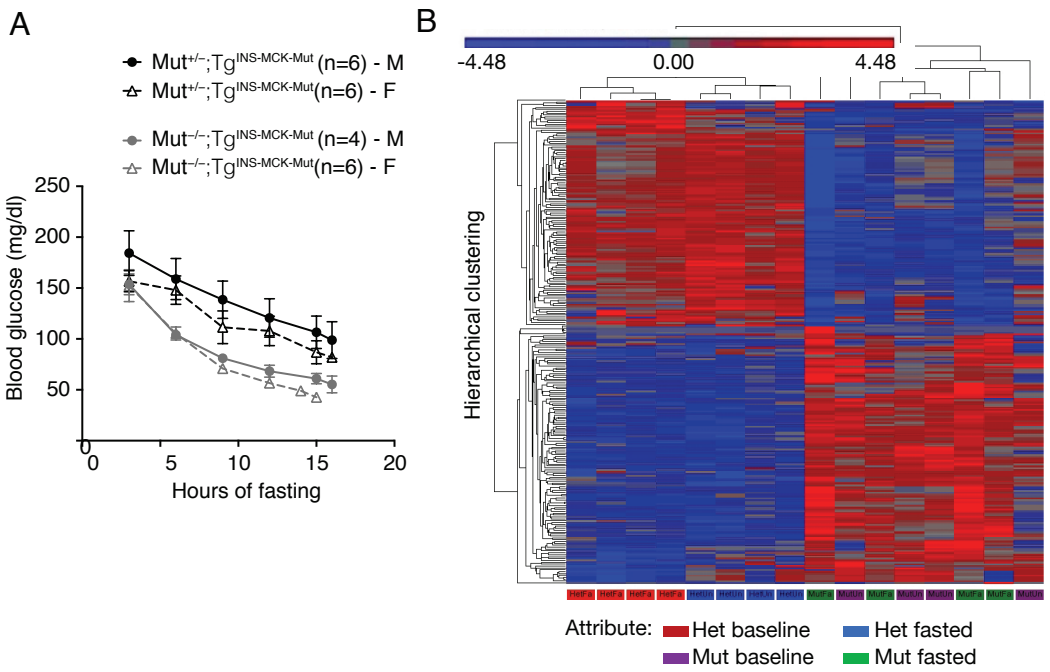

Fasting challenge.
(**A**) Blood glucose monitoring during the overnight fasting study in male and female *Mut*$^{-/-}$;Tg$^{INS\text{-}MCK\text{-}Mut}$ mice detected hypoglycemia in the smaller female mice after 15-16hrs of fasting. Mice were euthanized for tissue collection at this time point. (**B**) The dendrogram represents hierarchical clustering of genes with similar expression pattern in the microarray experiments in liver tissues. Genes upregulated in the *Mut*$^{-/-}$;Tg$^{INS\text{-}MCK\text{-}Mut}$ mice as opposed to control animals are indicated in Red and downregulated in Blue. Microarrays were performed in 2 groups of animals, mutant and control mice, in two conditions, baseline and fasting states. The scale (red to blue) represents the ratios of differential expression based on signal intensity.

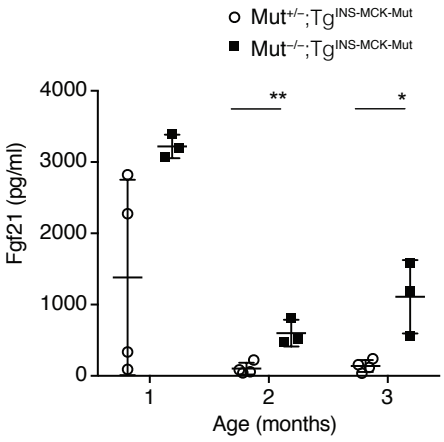

Longitudinal Fgf21 values.
(**C**) Samples obtained in a small number over time suggest that values are higher at weaning, even for some heterozygote animals, and then gradually increase after the first month in the mutant transgenic mice.

Supplemental Figure 7

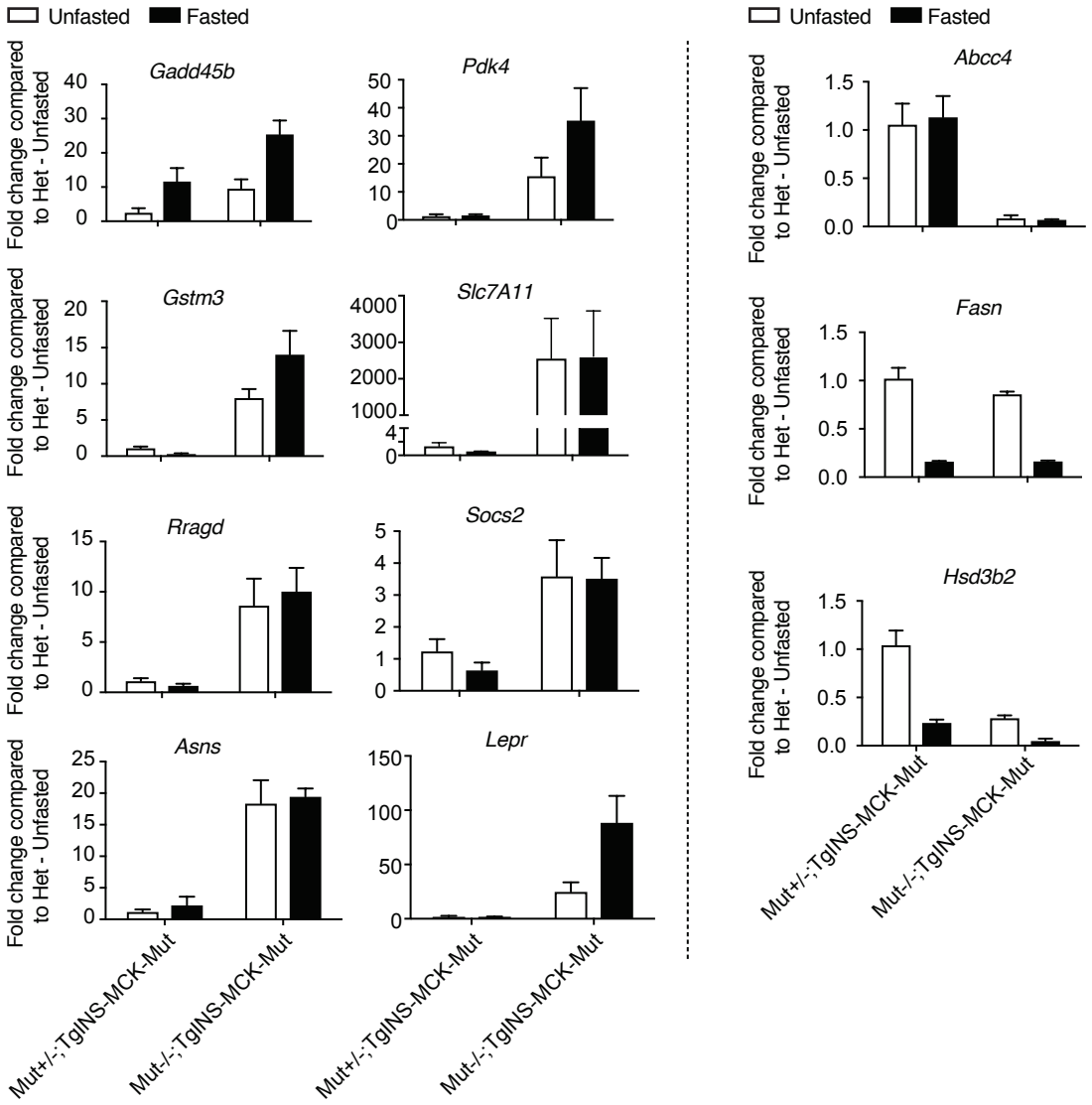

Validation of selected up- and down-regulated genes in the microarray experiment

Hepatic expression of selected genes in the unfasted and fasted state in heterozygote and mutant animals is depicted. An exaggerated response was often seen in *Mut*$^{-/-}$;Tg$^{INS\text{-}MCK\text{-}Mut}$ mice in several pathways (for example: *Gadd45b, Pdk4*), while for others a divergent response was observed, with genes that are normally downregulated being significantly induced (*Gstm3, Slc7A11, Rragd).* Downregulation of *Fasn* and *Hsd3b2* was consistent between *Mut*$^{-/-}$;Tg$^{INS\text{-}MCK\text{-}Mut}$ and their heterozygote littermates.

Supplemental Figure 8

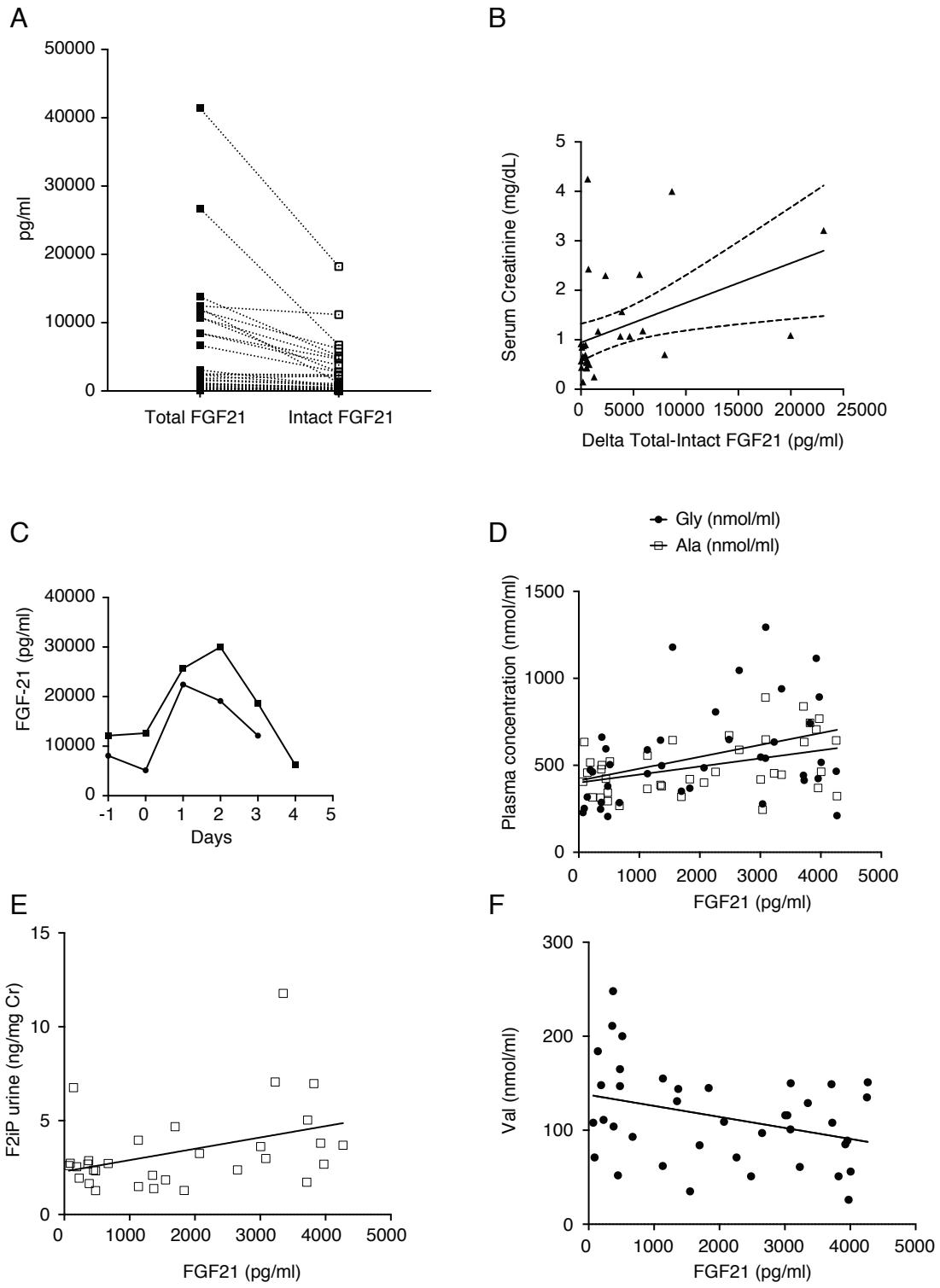

Plasma total and intact FGF21 and correlations with other biochemical parameters.
(**A**) Total and intact (active) FGF21 were measured in the same samples (N=38). Intact FGF21 ranged from 33.92 to 18,235 pg/ml (2,262 ± 3,636, mean ± SD). (**B**) Delta Total-Intact FGF21 showed a weak correlation (R^2=0.18, r=0.42, P=0.014) with renal function. **(C)** Serial FGF21 measurements before, during and after a metabolic crisis in two MMA siblings showed massive temporary increases in serum FGF21 concentrations that returned to pre-crisis levels upon recovery. (**D**) Plasma FGF21 correlated positively with plasma amino acids (glycine: r=0.36, P=0.0227, R^2=0.132 and alanine: r=0.41, P=0.0079, R^2=0.175, solid circles vs. clear square symbols, respectively), as well as (**E**) with urinary F2-isoprostanes (r=0.39, P=0.03, R^2=0.154). (**F**) There was a negative correlation with plasma valine (r=-0.345, P=0.03, R^2=0.12).